Journal of Power Sources 196 (2011) 9419–9428

Contents lists available at ScienceDirect

Journal of Power Sources

journal homepage: www.elsevier.com/locate/jpowsour

Improving the operation of a fuel-cell power unit with supervision control – A simulation study

Boštjan Pregelj[a,b,*], Darko Vrečko[a,b], Vladimir Jovan[a,b]

[a] Jozef Stefan Institute, Jamova 39, 1000 Ljubljana, Slovenia
[b] CO NOT, Hajdrihova 19, 1000 Ljubljana, Slovenia

ARTICLE INFO

Article history:
Received 6 May 2011
Received in revised form 20 June 2011
Accepted 22 June 2011
Available online 29 June 2011

Keywords:
Fuel cell power unit
Modeling
Supervision control
Efficiency
Degradation
Simulation

ABSTRACT

Polymer electrolyte membrane fuel cells are proving to be a clean and efficient source of energy. Nowadays, extensive research efforts are being focused on bringing this technology to everyday use. An important aspect when integrating fuel cells in practical applications is their ability to respond to load demand. With respect to this, due to their complex internal dynamics, fuel cells belong to the group of more slowly responding sources. In order to make them more generally applicative they are often connected with a battery or a super-capacitor via a power converter to form a hybrid power source. A control algorithm, designed for such a system, represents an interesting challenge: it has to adapt to varying working conditions and operate optimally in terms of efficiency and reliability, while minimizing any impacts on the degradation of the components. Here, we present an approach using supervisory control automaton that switches between the system's operational modes and sets the references for the lower-level control loops. The evaluation of the efficiency and degradation is carried out in a simulation using a model of the widely used 1.2-kW Ballard Nexa power module.

1. Introduction

Fuel cells with a membrane made from a polymer material (*Polymer Electrolyte Membrane fuel cells,* PEM FC) are a clean and efficient source of electrical energy [1–3]. However, despite the first practical implementations dating back to the era of manned flights into space in the early 1960s, they have only recently become the subject of intensive study and application; in particular in the fields of mobile applications, uninterruptible power-supply systems, auxiliary power units and vehicle drives. The main advantages of fuel cells are that the energy storage is in the form of hydrogen (so the energy is not lost over time), a high efficiency, a low operating temperature and a high power density [4,5].

In a FC stack there is an ongoing exogenous electrochemical reaction, where hydrogen and oxygen (from the air) are transformed into water; at the same time energy is released in the form of produced electricity and heat. Fuel cells behave as a current source, where the load current defines the reactant consumption and, consequently, the operating conditions, while support systems have to ensure that both reactants are supplied in sufficient quantities. If this is not the case, there is a high risk of an irreversible deterioration [5] of the cell membrane's functionality, which will eventually lead to failure. Therefore, the fuel-cell control algorithm has to adapt to the varying operating conditions and at all times operate optimally in terms of efficiency, reliability, and the health of the system, so as not to damage the stack or shorten its lifetime. An in-depth discussion on various approaches and solutions to stack control is given in [6], while some other advanced approaches are presented in [7,8].

An important aspect of introducing fuel cells into daily use is their ability to respond to the user's demands. In this respect, fuel cells belong to the class of slow-response energy sources because of their complex internal dynamics, related to mass- and thermal-equilibrium laws inside and around the stack. For certain applications this poses no problems (electromotor, forklift, etc.); however, very often this is not the case. To increase its range of functionality a fuel-cell stack is usually combined with a battery (or super-capacitor) into a hybrid power source [9]. Such a power-generation unit also consists of air (oxygen) and hydrogen supply subsystems, temperature and humidity control subsystems and a DC/DC converter [10]. During operation the battery (or super-capacitor) is used to sustain the current peaks that are a consequence of the changes on the load side, while the stack is controlled to provide the right power at the right time; the control actuator being a DC/DC converter, which adapts its output voltage to produce the required currents. A number of studies discussing the control of such systems are presented in [5,9–12].

Some studies follow the two-converter solution, where they adapt the voltage of the battery and the stack to the voltage of

* Corresponding author at: Jozef Stefan Institute, Jamova 39, 1000 Ljubljana, Slovenia. Tel.: +386 14773698; fax: +386 14773994.
E-mail address: bostjan.pregelj@ijs.si (B. Pregelj).

0378-7753/$ – see front matter © 2011 Elsevier B.V. All rights reserved.
doi:10.1016/j.jpowsour.2011.06.077

Nomenclature

DC	direct current
FSM	finite state machine
HV	heating value
K_p	proportional gain – parameter of PI/PID controller
MOMI	magnitude optimum multiple integration
SOC	state of charge
T_i	integral time – parameter of PI/PID controller
T_d	differential time – parameter of PID controller

Greek symbols

λ	oxygen excess ratio
η	efficiency
φ	mass flow

Subscripts

aux	auxiliary, i.e., losses
batt	battery
comp	compressor (blower)
DCDC	DC/DC converter value
deg	degradation
err	error
lim	limit/saturation value
meas	measured value
net	nett value
ref	reference value
stack	stack value

the bus [11], while other approaches [9] (including the one presented here) assume just a single converter between the stack and the other elements. This partly restricts the applicability due to the somewhat varying output voltage; however, it has other important advantages: simpler control, lower price and fewer losses.

In this work a control approach is proposed for the complete system. It is designed both to coordinate the operation of all the components and to optimize the system's sustainable functioning in terms of high efficiency, safety, reliability and durability [13,14]. The control is divided into high- and low-level control, where the high-level algorithm collects the process data, defines the current state of the system and sets references for the low-level control loops. An advantage of the described control in comparison with others is its low complexity and the fact that a model of the system is not required for tuning.

The paper presents a simulation system model, consisting of a stack, a DC/DC converter, a battery and an electric load. Furthermore, a control approach is presented, with a description of the high- and low-level control algorithms. The proposed control strategy is evaluated in a simulation, where the results are also compared to another control strategy. The comparison is summarised with a discussion relating to the overall efficiency and the stack-degradation measures.

2. Extended model of a FC hybrid power-generation unit

For the purpose of improving the operation of a complete system a model of the system can be used. Such a model should consist of all the elements in the energy production–distribution chain, i.e., a stack model, a power-converter model, a battery and a load. The scheme of the complete power system is shown in Fig. 1.

2.1. Model of a FC power-generation unit

For the analysis and the stack control design a model [15] of a 1.2-kW Ballard Nexa power-generation unit [16] was used. The Nexa is widely used in academic institutions and therefore interesting to use for the purposes of a comparison. The model, which fits the real data very closely, is implemented in Matlab–Simulink and allows a precise study of the system states and operation.

During normal operation of the stack a (load-dependent) sufficient supply of reagents (O_2, H_2) has to be provided. Hydrogen is stored in a high-pressure bottle or metal-hydride tanks; its flow control is defined by a mechanical ratio control that takes into account the required air flow, and is, therefore, treated as always sufficient. The oxygen (from the air) is supplied by a blower that feeds air into the stack, and which can be described as the first control input. However, for technical reasons, it has to be provided in excess [5] with respect to the chemical equation:

$$2H_2 + O_2 = 2H_2O + \text{electrical energy} + \text{heat} \quad (1)$$

Therefore, an oxygen-excess ratio λ is defined as:

$$\lambda = \frac{\text{input } O_2}{\text{reacted } O_2} \quad (2)$$

The optimal λ value is dependent on the stack current and is usually greater than 2. It has a lower critical boundary at $\lambda = 1$ – below this oxygen starvation is observed, leading to cell degradation and, eventually, failure. On the upper side there is no fixed limit; however, for higher values of λ the compressor requires more power than is gained by the stack and so the output power decreases.

The air is also used to humidify the membrane. To ensure the air brings enough water it has to be either humidified or taken to a temperature where its relative humidity is sufficient.

The stack has two further control inputs. Namely, during the operation, besides the electrical energy, heat is also produced. The optimal stack operating temperature is around 60–65 °C [16], and the surplus of heat energy needs to be taken away by a cooling fan – the second control input. Furthermore, as indicated by Eq. (1), the water is being generated on the oxygen (cathode) side. This side is open, i.e., there is a blower that is blowing air through the stack to an exhaust where the water is released. However, water is also condensing from the humidity on the hydrogen (anode) side. The hydrogen side is a dead end and the accumulated water has to be ejected by repeatedly opening the hydrogen purge valve, i.e., the third control input.

The stack model makes it possible to realise the three described control loops, as shown in Fig. 2, i.e., the water purge valve control, the temperature control and the oxygen excess ratio control (via the compressor voltage). The system has a humidifier, and therefore the

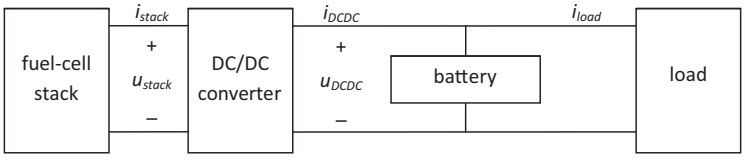

Fig. 1. Scheme of the complete power system – power-generation unit and load.

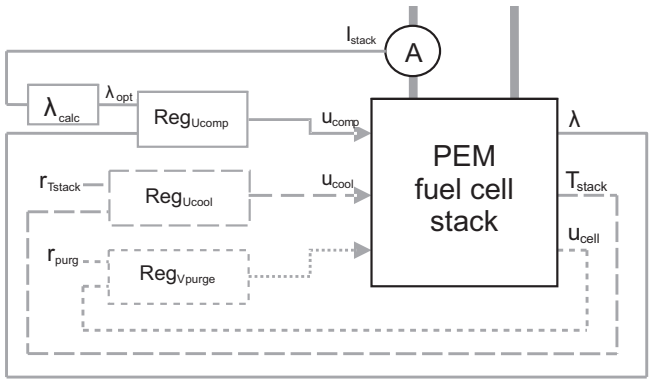

Fig. 2. Stack control scheme consisting of three main control loops: the air-blower control (full line), the cooling/temperature control (dashed), and the water-purge control (dotted).

humidity can be assumed to be at 100%. A comprehensive system analysis is given in [17] and the following section briefly presents the results.

2.1.1. Power characteristics of a fuel-cell stack model

The basic fuel-cell power-generation unit consists of several subsystems, which are all, except for the stack, direct consumers of power. The largest two power consumers are the air blower and the cooling fan. Therefore, during a calculation of the net output power one has to estimate the power losses, often called the *parasitic losses* or the *auxiliary power*. An estimate for the auxiliary power is proposed in [7], while in this work the following estimate was used:

$$P_{aux} = 0.27u_{comp} + 7.29 \times 10^{-3}u_{comp}^2 + 1.72 \times 10^{-4}u_{comp}^3 \quad (3)$$

where u_{comp} is the blower voltage. The stack unit output power can then be calculated from

$$P_{net} = P_{stack} - P_{aux} \quad (4)$$

where P_{stack} is the stack power, P_{aux} is the parasitic loss (auxiliary) power and P_{net} is the unit's output power.

To determine the power characteristics, several simulation experiments under various loads over the whole operating range were made. During each simulation the blower voltage was gradually decreased, from 100% to 30% in steps of 5%. The results show that by increasing the blower speed at constant load (i.e., increasing λ), the stack power exponentially ($1-k^{-\lambda}$) limits its maximum. However, an increase of the blower voltage causes an increase in the parasitic losses. Therefore, the output power characteristics at a constant stack current have a maximum. The complete range of static characteristics is plotted in Fig. 3. The results are similar to those already presented in [5].

2.1.2. Efficiency of a fuel-cell stack model

The fuel-cell stack efficiency is defined as the ratio of the electrical power generated by the stack to the power generated by burning the same amount of hydrogen [18]

$$\eta_{stack} = \frac{P_{stack}}{\phi_{stack\_H_2} HV} \quad (5)$$

where P_{stack} is the stack power, $\phi_{stack\_H_2}$ is the theoretical flow rate of hydrogen to the stack, and HV is the heating value of the hydrogen. In our case the hydrogen's higher heating value (High $HV_{H2} = 141900\,\mathrm{J\,g^{-1}}$) was used as most of the generated water is liquefied. A small amount of hydrogen is not consumed in the reaction

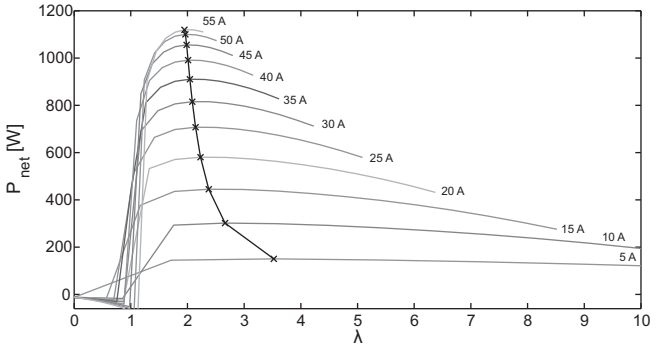

Fig. 3. Stack output power with respect to the oxygen excess ratio λ, drawn for different stack currents. The points of maximum output power are marked by X.

(due to the crossover effect [2,3] or leakage into the surroundings) and a modified equation can be used in the efficiency computation

$$\eta'_{stack} = \frac{P_{stack}}{(\phi_{stack\_H_2} + \phi_{stack\_loss}) \cdot HV} = \eta_{stack} \frac{\phi_{stack\_H_2}}{\phi_{stack\_H_2} + \phi_{stack\_loss}} \quad (6)$$

where ϕ_{stack_loss} is the flow of the actual hydrogen losses. The net efficiency is then calculated as:

$$\eta_{net} = \frac{P_{net}}{\phi_{supplied\_H_2} HV} \quad (7)$$

where P_{net} is the net output power, and $\phi_{supplied\_H_2}$ is the supplied H_2 flow rate. In Fig. 4 the calculated characteristic of the stack efficiency with respect to the stack current is shown, indicating the highest efficiency operating point near $I_{stack} = 20$ A, and stays at close to the maximum over a fairly wide range of current values.

2.2. Simplified power-converter model

There are two common types of DC/DC power converters: the first type gives a lower voltage at the output (buck converter) and the second gives a higher output voltage (boost converter). There are also more complex and expensive converters capable of both (buck-boost) conversions. In our case a buck converter was used since the stack voltage (26–43 V) is always higher than the required battery voltage (24 V).

Because of the faster dynamics, by several orders, of the power converter compared to the other components in the system, a simplified, lumped model of a DC/DC converter can be used:

$$d = \frac{U_{out}}{U_{in}}; \quad \mu = \frac{P_{out}}{P_{in}} = \frac{I_{out}\,U_{out}}{I_{in}\,U_{in}} \quad (8)$$

where d is the converter duty cycle, also representing the output/input voltage ratio (controlled input), and μ is the presumed constant converter efficiency of 95%. P, U and I represent the power, the voltage and the current on the stack (*in*) and the load (*out*) side of the converter.

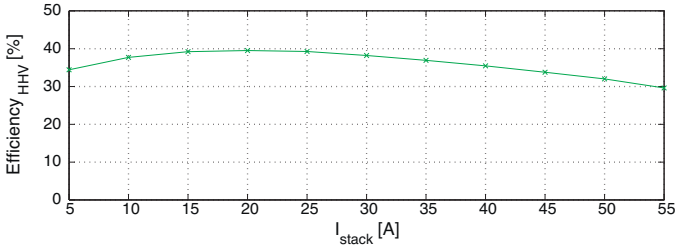

Fig. 4. Efficiency characteristics of a simulated FC stack model.

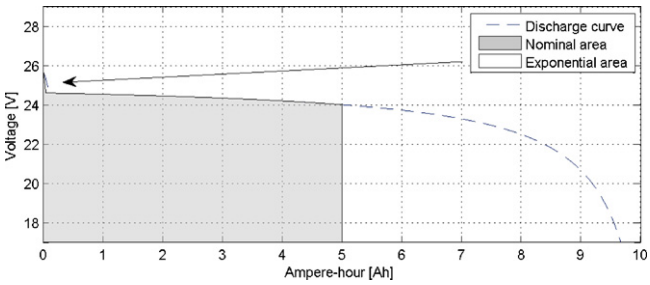

Fig. 5. SOC characteristic of the employed lead-acid battery model (Matlab/Simulink, Sim Power Systems).

2.3. Battery model

In our case a lead-acid battery model from the *Sim Power Systems* model library in the Matlab/Simulink environment was used [19]. The model gives the battery voltage as a function of the input/output currents

$$U_{batt} = E - I_{batt}R_{batt}; \quad E = E_0 - K\frac{Q}{Q - it} + A^{-B\cdot it};$$

$$it = \int_0^t I_{batt}d\tau, \tag{9}$$

where U_{batt} is the battery voltage, I_{batt} is the battery current (out), R_{batt} is the internal resistance, E is the no-load battery voltage, E_0 is the nominal voltage, Q is the battery capacity, K is the polarization voltage, A is the exponential voltage and B is the exponential capacity.

The model also estimates the battery's state of charge (SOC), given as

$$\text{SOC} = 100\left(1 - \frac{\int_0^t I_{batt}d\tau}{Q}\right) \tag{10}$$

In our case the following nominal values were used: $Q = 10$ A h, $E_0 = 25.29$ V, $R_{batt} = 0.06$ Ohm, $A = 1.32$, and $B = 375$. The static characteristic of the battery model is shown in Fig. 5. In practice, the battery capacity is chosen based on the stack and load-demand specifications.

2.4. Load model

The load may be generally described by considering its purpose of use. The latter defines the energy-use profile and, consequentially, the source specification. In general, we identify the following types of use:

- Uninterruptible power supply (UPS).
  - o Important fast start-up, power demand typically constant.
- Auxiliary power unit (APU), where no other source is present.
  - o Adaptation to variable load – variation across whole operating range should not affect the unit's life-time.
- Mobile unit's/drive power supply (vehicle, car, forklift, etc.).
  - o Possibility of a direct connection of the stack to the load (no conversion necessary).

In our case the variable load was simulated using a current generator with instantaneous switches, as the unpredictable on/off switching of several power consumers, which is often the case with APUs.

3. Control design for the extended system

Designing a control scheme for the entire system requires a decision on the hierarchy of the control objectives. The control scheme should comprise three control loops: (a) charging the battery, (b) adjusting the converter's output voltage, and (c) blowing air into the stack. It has been shown in [20,21] that the high voltage at the stack output, which translates into a high voltage on the individual cells, accelerates the growth of the catalyst particle size, consequently reducing its active surface. At the same time, it is important to monitor the lowest cell voltage, which must not fall below 0.5 V per cell. In such a case it is possible that we obtain a negative voltage on one of the cells, and consequently a greater voltage on the neighbouring cells, which again leads to cell deterioration. In addition, we tend towards a smooth change of the stack load and operation in the range with the highest efficiency. Regarding the chosen battery type, the desired control goals are as follows: a state of charge (SOC) between 40% and 80%, charge/discharge currents within the required limits and optimization of the number of charging cycles.

The above-mentioned requirements lead to a two-level control scheme. On the higher level there is an advanced supervisory control algorithm, using the on-line measurements of both the battery SOC and the actual load current (I_{load}), which calculates a reference for the stack current (I_{stack_ref}) with two goals: maximizing the efficiency and ensuring the sustainable operation of the entire system. At the lower level, two controllers are used. First, the DC/DC converter controller controls the ratio d, which affects the converter output voltage, u_{DCDC}. The voltage difference (u_{DCDC}–u_{batt}) creates the current from the converter to the battery, which further results in the current from the stack (I_{stack_ref}). The second lower-level controller controls the air blower so as to maintain the appropriate oxygen excess ratio in the stack operation. The scheme of the proposed control system is presented in Fig. 6.

3.1. High-level coordination control

For the supervisory control algorithm we propose a control strategy based on four regimes of stack operation

- OFF – stack shut down.
- LOW – stack operates at low power.
- NORMAL – stack operates at the highest-efficiency working point.
- POWER – stack operates at high power.

The switching among all the above-mentioned regimes is conditioned by considering the instantaneous state of the battery (charge = CHG/discharge = $\overline{\text{CHG}}$), the battery SOC and the load current. In practice, the system mostly operates in the NORMAL regime at the optimal working point ($I_{normal} = 20$ A), as described in Section 2.1.2. The LOW mode ($I_{low} = 10$ A) is introduced to prevent switching on and off too often in the case of low demand. Only in the case of a high load current and a low SOC value is the stack switched to the POWER regime, where the stack current reference is set in accordance with the actual load current as $I_{stack\_ref} = \min(I_{load}, 45\text{ A})$; consequently, with a lower efficiency and possible degradation effects being present. In general, also in this regime, the system tends towards the lowest possible stack-current values.

The state-transition diagram of a high-level coordination algorithm is depicted as a finite state machine (FSM) in Fig. 7. Furthermore, considering the load specifics and its time profile, it is possible to set additional time conditions with respect to the switching among the FSM states, i.e., the system's operating modes. The actual stack-current reference is changed following a ramp profile. In this way, smooth transitions are achieved, ensuring that the blower supplies a sufficient amount of air to the stack at all times.

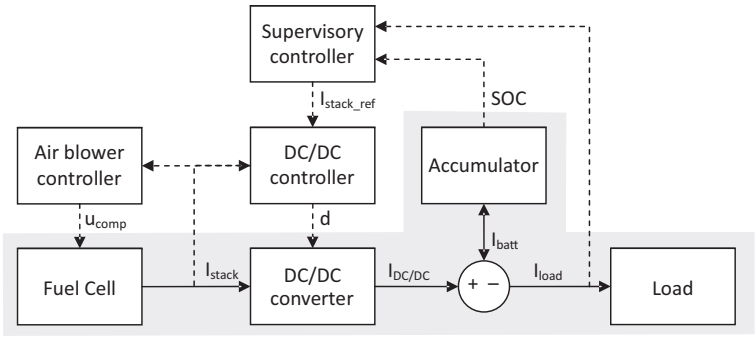

Fig. 6. Two-level control scheme of the extended fuel-cell system model; the power elements have a gray background; the full lines represent current flows; and the dashed lines represent control signals.

3.2. Low-level control–DC/DC converter control

The element that influences the battery charging and the stack load is the DC/DC power converter. As explained in 2.2, by varying the input/output voltage ratio d, its output voltage (U_{DCDC}) is controlled so that, consequently, the desired current I_{stack} is drained from the stack. In our case the I_{stack} PI control law is as follows

$$d = K_p(I_{stack\,err} + \frac{1}{T_i}\int_0^t I_{stack\,err}d\tau) - \frac{K_p}{T_i}\int_0^t (d - d_{\lim})d\tau,$$
$$K_p = 0.31, \quad T_i = 1.148\,\text{s} \tag{11}$$

where I_{stack_err} is the difference between the measured value I_{stack} and its reference value (I_{stack_ref}). Given the limited range of d values (d_{lim} is represented by 0 and 1) the anti-windup protection is introduced, shown in the last part of the equation. The controller was tuned using the MOMI method for PI controllers [22] with some manual fine-tuning. In this way, the controller is tuned with the off-line-generated, open-loop, step-response control data using multiple integrations.

3.3. Low-level control–air-blower control

A sufficient air supply is vital for the stack's operation. In order to optimize the operation, the compressor is used to adjust λ towards the desired value; the control scheme of the air supply is shown in Fig. 8.

The reference λ value of the air-supply control varies regarding the stack current based on the maximum power points shown in the characteristics in Fig. 3. The nonlinear static dependency of the optimum points, given in Table 1, is presented in Fig. 9.

The characteristic curve is used for the reference λ value calculation for the compressor control to minimize the losses and use the stack at the safest power levels. For λ tracking control a PID controller with the following control law was used:

$$U_{comp} = K_p(\lambda_{err} + \frac{1}{T_i}\int_0^t \lambda_{err}d\tau + T_d\frac{d\lambda_{err}}{dt}) - \frac{K_p}{T_i}\int_0^t (u_{comp} - u_{comp\_\lim})d\tau, \tag{12}$$

where λ_{err} is the error between the reference and the estimated value of λ, and the controller parameter values are $K_p = 6$, $T_i = 2/3$ s, $T_d = 1/15$ s. Due to the limited operating range of the compressor voltage (0–100%), the anti-windup protection is also used here. The controller was tuned using the MOMI method for PID controllers [22] with some experimental fine-tuning.

The nonlinearity of the λ characteristic curve would normally cause control problems; therefore, it is important to point out that the effect is far more expressed in the lower part of the operating range. As mentioned above, we try to avoid operating at low currents as much as possible anyway, as it may lead to a deterioration of the stack's performance [20]. Thus, the controller may be tuned to operate best in the medium-high operating range.

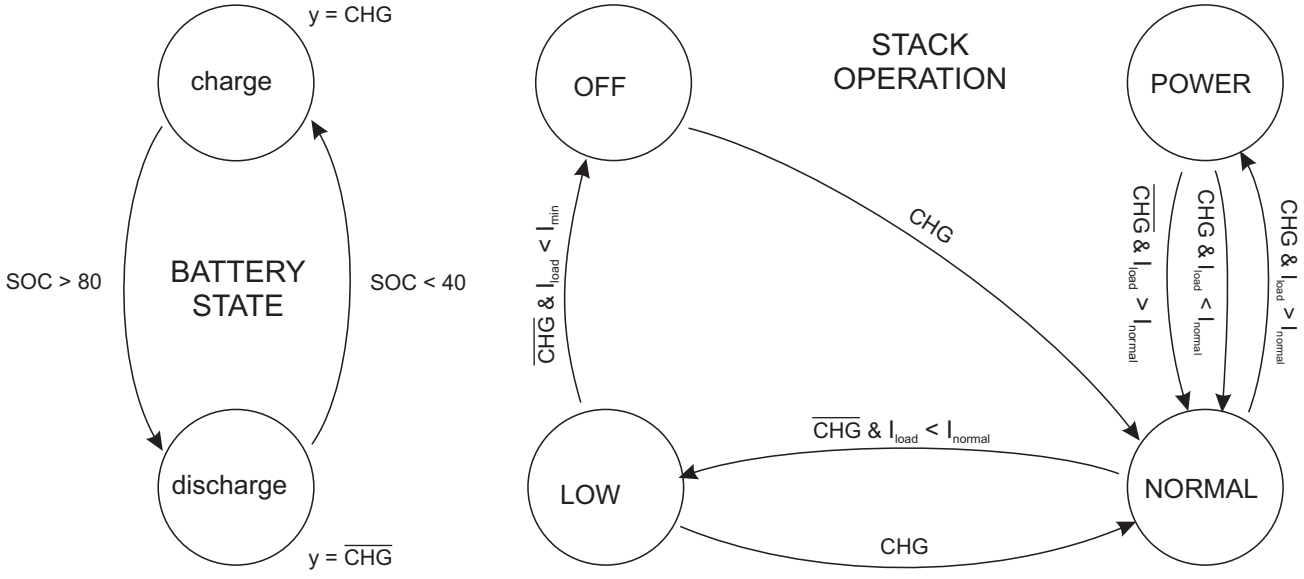

Fig. 7. Regimes and conditions of the proposed (Finite State Machine) high-level controller.

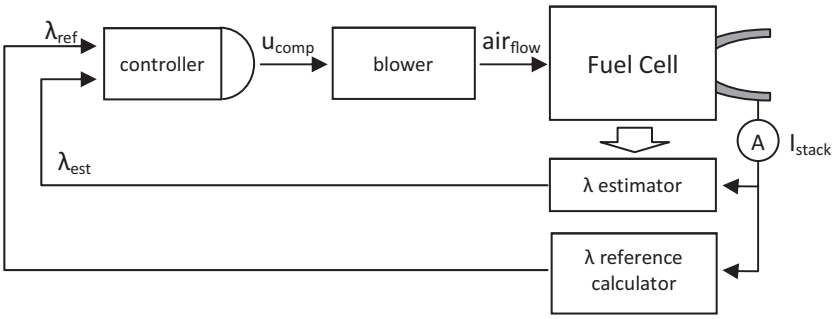

Fig. 8. Air-supply control scheme.

Table 1
Static dependency of optimum λ values according to the stack current (I_{stack}).

I_{stack} (A)	5	10	15	20	25	30	35	40	45	50	55
λ	3.522	2.662	2.375	2.230	2.143	2.084	2.042	2.010	1.985	1.965	1.947

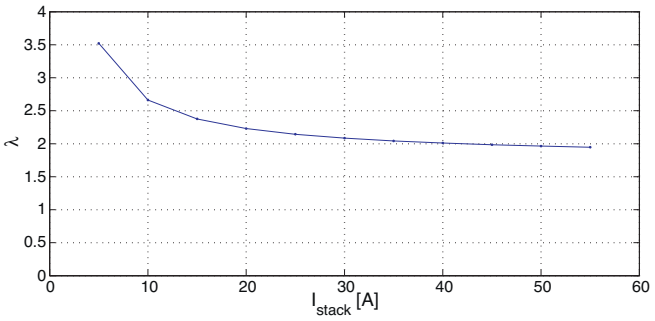

Fig. 9. Optimum λ values for the entire stack operating range.

Fig. 10 shows the time plot for the stack signals for the varying load profile in the upper diagram, for a safe value $\lambda_{ref} = 3$ (gray line) and for a power optimized $\lambda_{ref} = \lambda_{opt}$ (black line), where a linear interpolation between the λ_{opt} points from Table 1 is used. Using λ_{opt} values in a control algorithm, a slightly higher net output power in the second diagram and a higher net efficiency in the third diagram can be observed, especially in the higher-power operating range. However, in both cases the key control problem is providing a sufficient quantity of air at the transients, where the consumption/load is suddenly increased, and consequently λ may temporarily fall below the critical value of 1, as happens at 1500s.

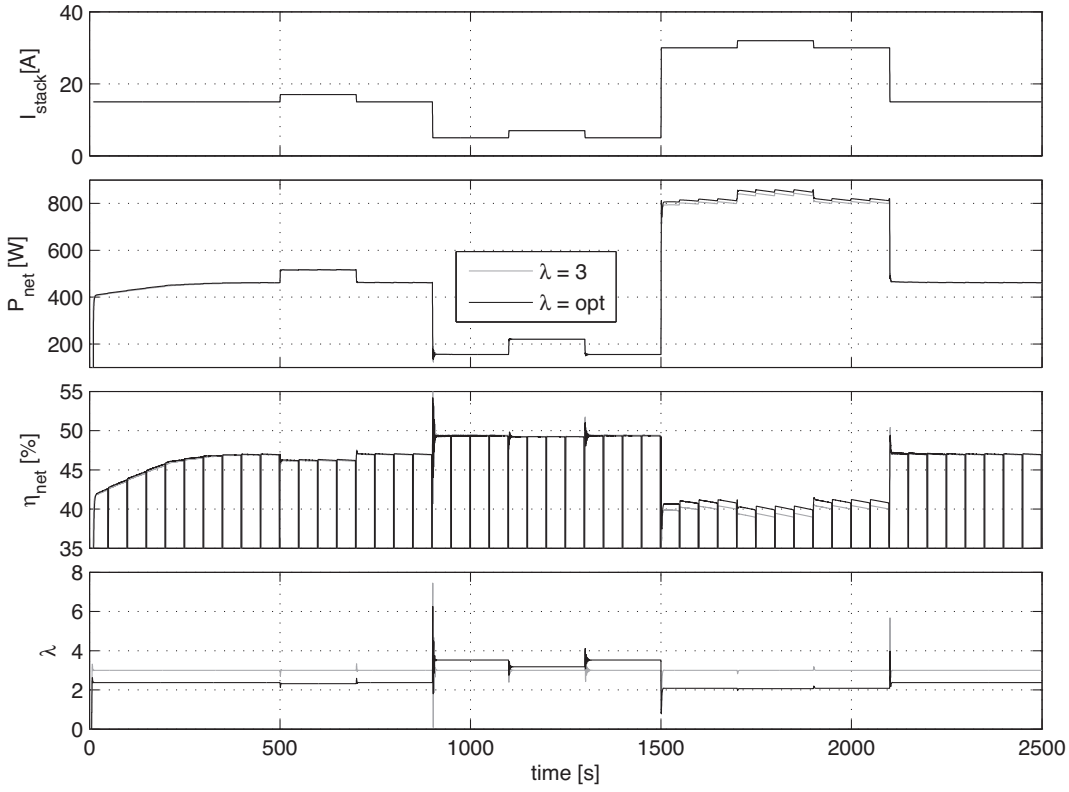

Fig. 10. Stack control with a variable load profile for reference λ = 3 (gray) and λ = λ_{opt} (black). Diagrams top-down: (1) stack current, (2) net output power, (3) net efficiency and, (4) oxygen excess ratio λ.

Table 2
Operating conditions' impact on stack degradation for a 1.2-kW Nexa power unit produced by Ballard.

Operation	Conditions	Degradation Rate	Period	Losses
Steady-state	Full power (46 A_{net})	$-25\,mW\,h^{-1}$ $-0.54\,mV\,h^{-1}$	1500 h	−37 W −0.8 V
	Part load (<35 A_{net})[a]	$-0\,mW\,h^{-1}$ $-0\,mV\,h^{-1}$	1500 h	0 W 0.0 V
Dynamic loads	Idle to full power	$-0\,mW\,h^{-1}$ $-0\,mV\,h^{-1}$	1500 h	0 W 0.0 V
On/off	Off – 46 A_{net}	$-52\,mW\,cycle^{-1}$ $-1.10\,mV\,cycle\,h^{-1}$	500 cycles	−26 W −0.56 V

[a] We considered that the losses increase linearly from 0 to 25 $mW\,h^{-1}$ (i.e., 0.54 $mV\,h^{-1}$) as the current increases from 35 A to a maximum of 46 A.

4. Criteria for evaluation of the proposed control

A useful comparison of energy sources can only be based on measurable quantities. Below we present the two criteria that will help us in assessing the overall quality of the control. These criteria are the stack efficiency and stack life-time degradation impact.

4.1. Stack efficiency

One of the key parameters for the stack-operation evaluation is efficiency. In this area the fuel cells, as an energy source, compete with others. To evaluate the efficiency, we used a simple measure – the integral of the ratio of the generated output electrical power (less the auxiliary power) and the power of burning the hydrogen fed to the stack (see Eq. (7)):

$$\eta_{overall} = \frac{1}{t}\int_0^t \eta_{net}\,d\tau \tag{13}$$

4.2. Stack life-time degradation

To assess the influence of the operating conditions on the deterioration of the stack's characteristics, we used the information from documentation [16] that the manufacturer provides for the 1.2-kW Nexa power unit. They have tested specific conditions for 1500 h and 500 off-to-full power cycles, for which the data are shown in Table 2.

Table 3
Degradation influence of the oxygen-starvation effect.

Operation	Conditions		Degradation rate
Steady-state	$\lambda < 1.0$	$\lambda = 1.0$[a]	$-0\,mW\,s^{-1}$
		$\lambda = 0.0$	$-10\,mW\,s^{-1}$

[a] We considered that the losses increase linearly from 0 to 10 $mW\,s^{-1}$ as the λ decreases from 1 towards 0.

As an additional degradation measure, the degradation rate for stack operation below the oxygen excess ratio $\lambda = 1$ was introduced, given in Table 3. Cell starvation is a very rigorous degradation phenomenon and therefore it is heavily penalized. This data is not given in the Nexa documentation as the embedded controller and DC/DC converter provided in the package work to avoid such conditions. The influence escalates linearly with the distance from value 1.

As an indicator in the control strategy comparison we used the cumulative sum of the performance losses due to operation in degenerating conditions over the simulation time.

$$P_{deg} = \int_0^t \left[\max\left(\frac{(I_{stack}-35)}{46-35}\frac{25\times10^{-3}}{3600},\,0\right) + \max\left(\frac{(1-\lambda)}{1-0}10\times10^{-3},0\right)\right]d\tau + n\times52\times10^{-3} \tag{14}$$

where P_{deg} is the cumulative power fall-off as a consequence of the degradation and n is the number of on/off cycles.

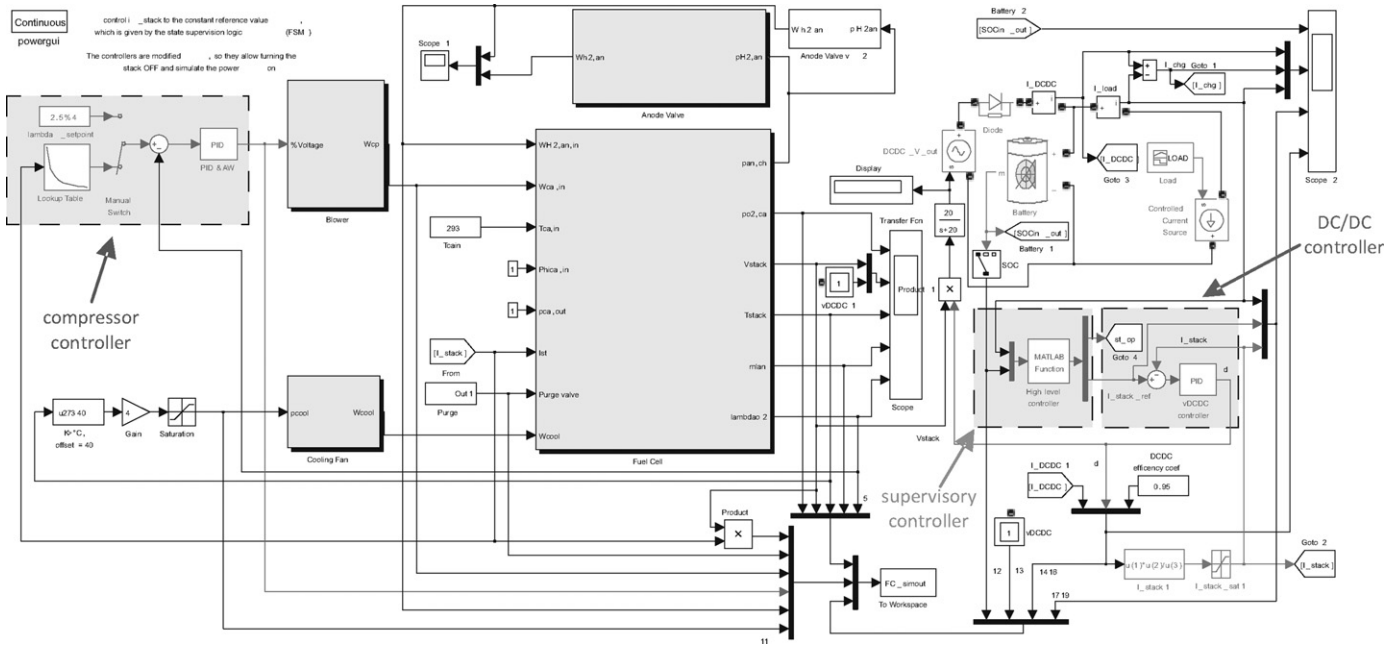

Fig. 11. Simulation scheme of the extended system model and control in the Matlab/Simulink environment.

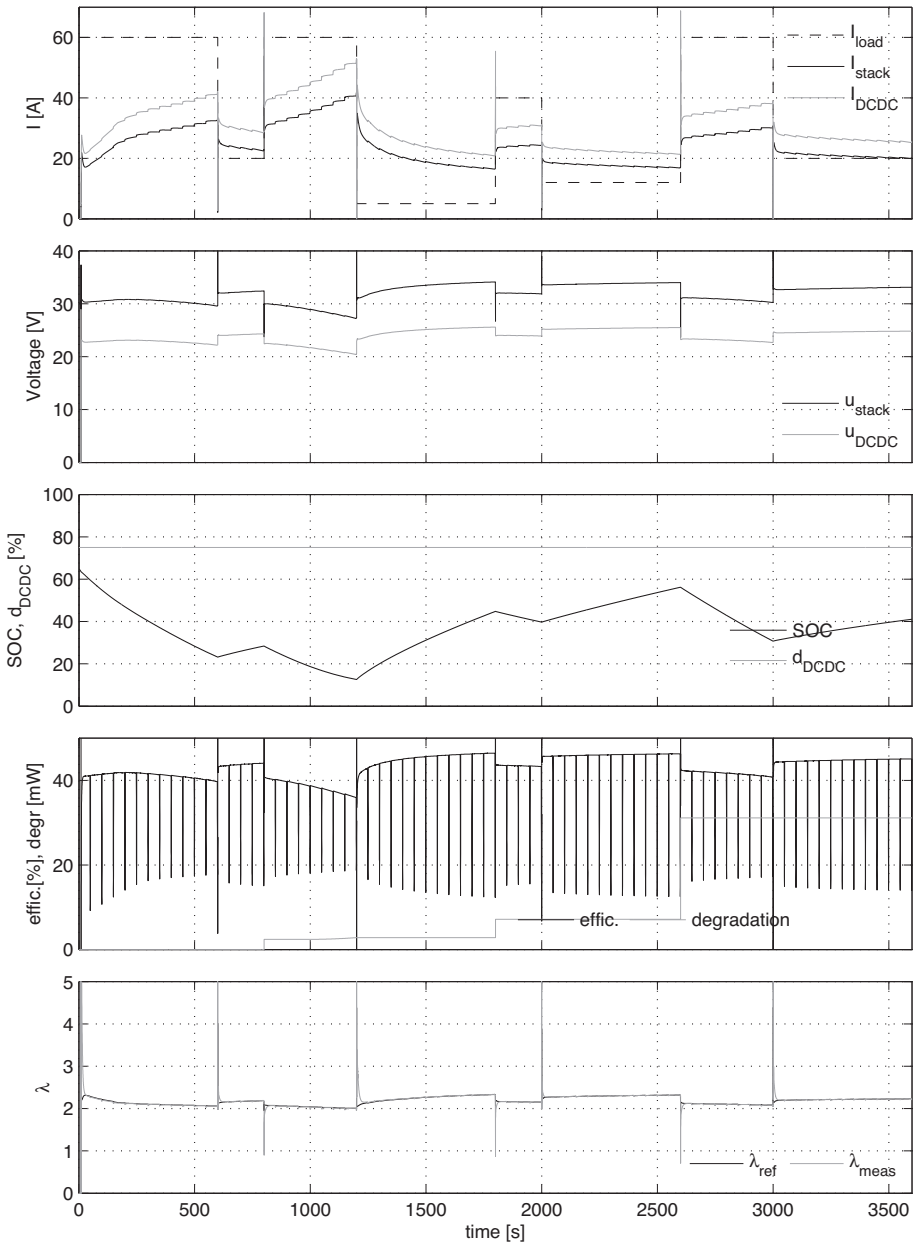

Fig. 12. Extended system-control time plot; a constant DC/DC converter transmission ratio $d_{DCDC} = 0.75$ is used. Signals top-down: (1) load current (dashed black), stack current (black), DC/DC out current (gray); (2) stack voltage (black) and DC/DC out voltage; (3) DC/DC transmission ratio d (gray) and battery SOC (black); (4) efficiency (black) and degradation (gray); (5) reference (black) and actual (gray) oxygen excess ratio values.

5. Control strategy analysis under a simulated load profile

The proposed approach of the extended FC system control was compared to another approach in a simulation where a constant value of the DC/DC power converter voltage ratio d is assumed. Its value is defined by the average ratio of the stack-to-battery voltage.

The simulation scheme of the extended model (presented in Section 3) and the proposed control system using Matlab/Simulink is shown in Fig. 11. In the simulation a smaller-capacity battery ($Q = 10$ A h) was used, so that in a reasonable time some interesting responses and transients could be observed.

In Figs. 12 and 13 the simulated essential signals of the evaluated control strategies are presented. The experimental load profile is plotted with a dashed line in the upper diagram. In Fig. 12 a simulation using a constant DC/DC conversion ratio ($d = 0.75$) is used. It can be observed that there is no direct control over the battery SOC (Diagram 3), and its value falls down to a critical level (12.6%) during a very high load; similarly, the overcharging problem arises with small loads. In addition the load variations (steps, transients) transform directly to stack-current spikes, resulting in λ (Diagram 5) falling below the value of 1 on certain occasions, consequently leading to stack degradation. On the other hand, the operating point is kept close to the optimal efficiency at all times.

In Fig. 13 the simulation using a control approach that is described in this work is presented. One can see that by using the DC/DC converter and battery it is possible to compensate for the current peaks and spikes caused by the load changes and achieve smoother, ramp-shaped transitions of the stack current. The stack is controlled to operate in optimal conditions whenever possible, only increasing the stack power in the case of large loads and decreasing it when the battery is highly charged and the load current is small.

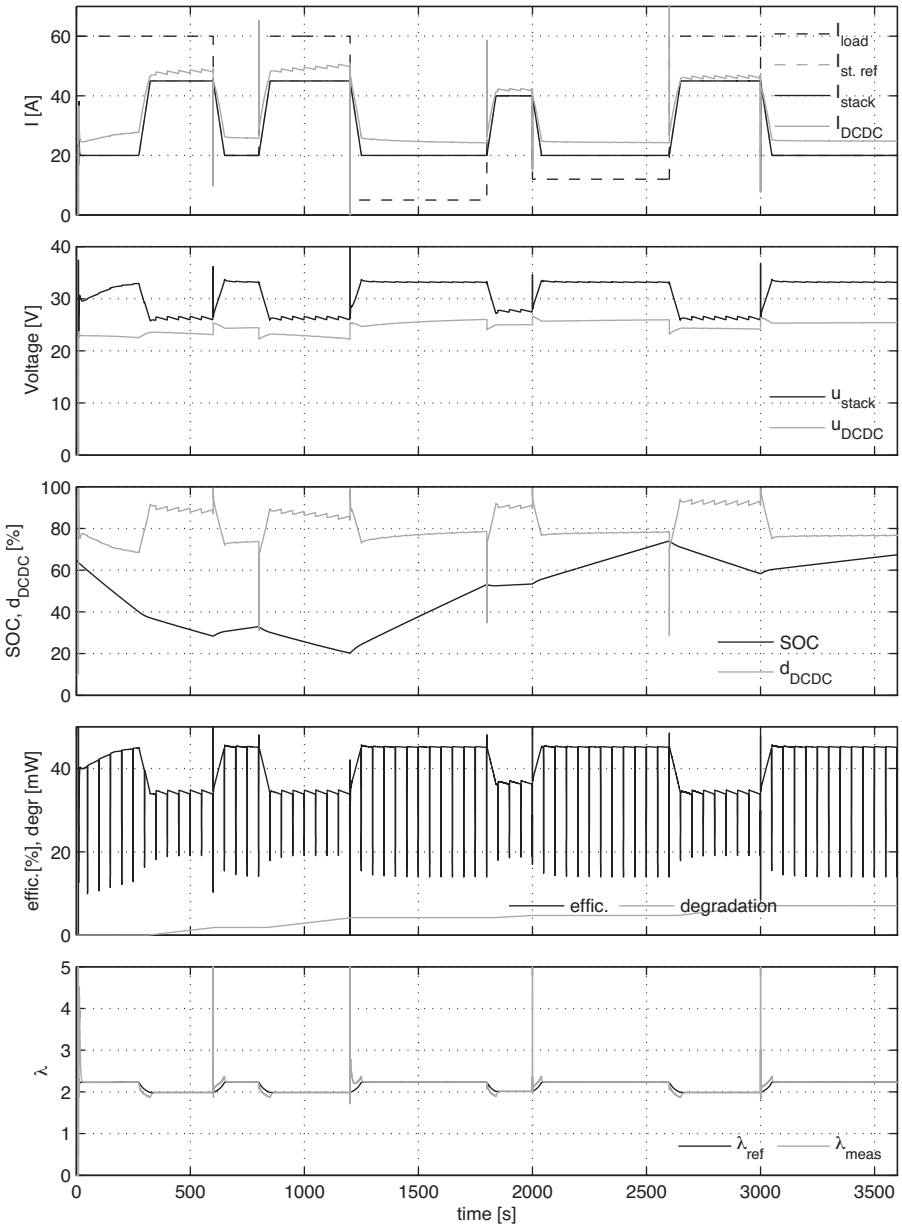

Fig. 13. Extended system-control time plot of the strategy that is presented in this work. Signals in the top Diagram (1) load current (dashed black), stack-current reference (dashed gray) and actual (black) value, DC/DC out current (gray). Signals in other diagrams as in Fig. 12.

The reader should note that the SOC values after the experiment are not equal for the presented control approaches. This is because the load profile was considered as an excitation signal only and the study focuses on the stack-operation parameters and the quality of the energy provided. The criteria values for the control strategies are given in Table 4.

6. Discussion

From these simulation experiments some interesting conclusions can be drawn. In terms of efficiency only, there is an advantage with the simpler approach using a constant d ratio over the control approach presented in this work. Using a constant d, a subtle closed-loop control function over the battery SOC is embedded. On average it causes the stack current to tend towards the appropriate constant value (see Fig. 12), provided d is set correctly, and the load profile has a constant long-term average. In the presented case the choice of $d = 0.75$ resulted in a lower final SOC value and a lower average output/load voltage compared to the supervisory control; by increasing the d ratio the efficiency would decrease. However, using constant d, the charging depends mainly on the instantaneous load and the SOC, so the desired charge/recharge cycles and SOC limits cannot be ensured.

This shows that by designing a sensible control function a balance between both approaches can be achieved, which would allow a further optimized operation to be achieved without sacrificing the safety of the components during operation. Another point to note is that including knowledge of the future load profile would

Table 4
Comparison of indicators for the tested control strategies.

	$d = 0.75$	FSM supervision control
Net stack efficiency	0.4099	0.3804
Stack degradation (mW)	31.1286	7.0773

make it possible to plan the operation closer to optimal conditions and bring additional gains in terms of efficiency maximisation and component-degradation reduction.

7. Conclusion

We present a model of a fuel-cell-based power-generation unit, consisting of the stack, a battery and a power converter. An advanced, two-level control approach is presented, consisting of a finite state machine for the high-level control and PID controllers for the low-level loops, which provides a good balance between optimal and reliable control, as well as a low computational complexity. This approach to the design of FC system control is compared to a simpler strategy and evaluated with efficiency and degradation criteria. The proposed control achieves a slightly smaller efficiency, but maintains the stack and the battery within the safe operating range. In future investigations, a more advanced control algorithm with a relatively simple model of the complete system will be developed and tested on a real system.

Acknowledgements

We thank the *Low-carbon Technologies Centre of Excellence* CO NOT, financed by the Ministry of Higher Education, Science and Technology and co-financed by the European Regional Development Fund for their financial support.

References

[1] F. Barbir, PEM Fuel Cells: Theory and Practice, Elsevier, 2005.
[2] S. Srinivasan, Fuel Cells – From Fundamentals to Applications, Springer Science-Business Media LLC, 2006.
[3] N. Sammes, Fuel Cell Technology, Springer Verlag, London Ltd., 2006.
[4] J.S. Lee, N.D. Quan, J.M. Hwang, S.D. Lee, H. Kim, H. Lee, H.S. Kim, Journal of Industrial and Engineering Chemistry 12 (2) (2005) 175–183.
[5] C.A. Ramos-Paja, C. Bordons, A. Romero, R. Giral, L. Martínez-Salamero, IEEE Transactions on Industrial Electronics 56 (3) (2009) 685–696.
[6] J.T. Pukrushpan, A.G. Stefanopoulou, H. Peng, Control of Fuel Cell Power Systems: Principles, Modeling, Analysis and Feedback Design (Advances in Industrial Control), Springer-Verlag London Limited, 2004.
[7] J.K. Gruber, M. Doll, C. Bordons, Control Engineering Practice (2009).
[8] J.K. Gruber, C. Bordons, F. Dorado, Proceedings of the American Control Conference, Seattle, USA, June 11–13, 2008.
[9] K.W. Suh, A.G. Stefanopoulou, International Journal of Energy Research 29 (12) (2005) 1167–1189.
[10] Z. Jiang, R.A. Dougal, Design and Testing of a Fuel-cell Powered Battery Charging station, 2009.
[11] A. Arce, A.J. del Real, C. Bordons, Journal of Process Control 19 (2009) 1289–1304.
[12] A.S. Sousir, A.H.M. Yatim, Simulation Modelling Practice and Theory 18 (2010) 663–676.
[13] P. Ruetschi, Journal of Power Sources 127 (2004) 33–44.
[14] J. Vetter, P. Novák, M.R. Wagner, C. Veitb, K.-C. Möller, J.O. Besenhard, M. Winter, M. Wohlfahrt-Mehrens, C. Vogler, A. Hammouche, Journal of Power Sources 147 (2005) 269–281.
[15] A.J. del Real, A. Arce, C. Bordons, Journal of Power Sources 173 (1) (2007) 310–324.
[16] Ballard, Nexa Power Module User's Manual, Ballard Power Systems Inc, 2003.
[17] B. Pregelj, D. Vrečko, P. Čufer, V. Jovan. Analysis of the fuel-cell system model for the control optimization, (JSI internal report, No.10414), 2010.
[18] V. Jovan, M. Perne, J. Petrovčič, Energy Conversion and Management 51 (2010) 2467–2472.
[19] Mathworks MATLAB/Simulink software and reference library.
[20] N. Yousfi-Steiner, Ph. Moçotéguy, D. Candusso, D. Hissel, Journal of Power Sources 194 (2009) 130–145.
[21] R.L Borup, J.R. Davey, F.H. Garzon, D.L. Wood, M.A. Inbody, Journal of Power Sources 163 (2006) 76–81.
[22] D. Vrančič, S. Strmčnik, D. Juričić, Automatica 37 (2001) 1473–1479.